Bull. Chem. Soc. Ethiop. **2025**, 39(5), 859-875.
DOI: https://dx.doi.org/10.4314/bcse.v39i5.5

ISSN 1011-3924
Printed in Ethiopia
Online ISSN 1726-801X

SYNTHESIZING, CHARACTERIZATION OF SOME METAL ION COMPLEXES WITH NEW AZO DYE AND STUDYING ANTIOXIDANT AND ANTICANCER (MCF-7)

Noor Talal Ali Al-Rubaye* and Abbas Ali Salih Al-Hamdani*

Department of Chemistry, College of Science for Women, University of Baghdad, Iraq

(Received December 17, 2024; Revised January 17, 2025; Accepted January 22, 2025)

ABSTRACT. This new azo dye 7-(3-hydroxy-phenylazo)-quinoline-8-ol was subsequently used to prepare a series of complexes with the chlorides of Fe, Co, Zn, Ru, Rh and Cd. The compounds identified by ^{1}H and ^{13}C-NMR, FT-IR, UV-Vis, mass spectroscopy, as well as TGA, DSC, and C.H.N., conductivity, magnetic susceptibility, metal and chlorine content. The results showed that the ligand behaves in a trigonal behavior, and that the complexes gave tetrahedral, except for Fe, Ru and Rh octahedral was given, that all of them are non-electrolytes. The effectiveness of both the compounds in inhibiting free radicals was evaluated by the ability to act as an antioxidant was measured using DPPH as a free radical and gallic acid as a standard substance, the IC_{50} value was determined, because the ligand was found to have a higher ability to inhibit free radicals, and the ability to inhibit the complex varied according to the IC_{50} value. Cobalt, zinc and ruthenium complexes were evaluated as anticancer agents breast cancer MCF-7 in five concentration, the results showed that the IC_{50} value for Zn was 43.38 µg/mL, while the ruthenium complex gave 63.57, cobalt complex gave 93.84 µg/mL, meaning that the Zn-complex gave a higher inhibition value than Ru and Co.

KEY WORDS: Antioxidant, Azo dye complexes, 8-Hydroxyquinoline, Anticancer

INTRODUCTION

The azo chromophore, which gives these compounds their distinctive colors, is present in one or more of the important class of organic chemical compounds known as azo compounds (-N=N-) [1]. Because of their numerous uses in several branches of chemical science and industry [2], azo dyes are the most widely used class of organic chemicals and have piqued the curiosity of many researchers. These dyes are used as dye materials in the polymer, leather, and pharmaceutical industries [3]. Azo-metal complexes are thought to be novel, inexpensive substances with a variety of antibacterial, anti-inflammatory, and anticancer properties [4, 5]. In drug development, this kind of complex is very important, particularly for metal-based anticancer medications [6, 7]. Natural or manufactured antioxidants are chemicals that can neutralize free radicals by working at multiple phases, such as prevention, repair, and interception [8, 9]. Therefore, the development of therapeutic medicines with enhanced potential for the treatment of a wide range of oxidant infections is required [10]. Through research, we did not find a previous study similar to our compound, according to a search in Science Finder. In this paper study is to mold the azo ligand H_2L into novel complexes of the metal ions Ru^{+3}, Rh^{+3}, Zn^{+2}, Fe^{+3}, Co^{+2}, Cd^{+2}. Their stability and thermal breakdown were investigated using DSC and TGA curves in addition to spectroscopic studies for characterization. Using the reference gallic acid, we also assessed the antioxidant properties of the Cd, Fe, Zn and Co complexes against the DPPH radical. Five concentrations of Co, Ru and Zn complexes were used in a study to assess their anticancer potential against MCF-7, and the IC_{50} was calculated.

*Corresponding authors. E-mail: noor.ali2305m@csw.uobaghdad, abbasas_chem@csw.uobaghdad.edu.iq

EXPERIMENTAL

Material and methods

The trading providers 3-Aminophenol, 8-hydroxyquinoline, NaOH, $ZnCl_2$, $CdCl_2$, $FeCl_3$, $CoCl_2.6H_2O$ [$RhCl_3.3H_2O$ and $RuCl_3.3H_2O$ Sigma Aldrich and ethanol, HCl conc., and DMSO Merck. (C.H.N.) were determined using Urovector model EA/3000, singleV3O. Mineral ions were identified as M-O using gravimetric methods. Molar conductivity was determined using conductivity meter W-T-W, 25 °C. 1×10^{-3} M. Solvents such as DMSO were used. Mass Spectrometry (MS) Q-P-50-A-D-I analysis mass spectra of various compounds were collected using a Shimadzu QP(E170Ev)-2010 Plus mass spectrometer. UV-Vis absorption spectra were obtained using a Shimadzu UV-1800 spectrophotometer. ^1H and ^{13}C NMR spectra were obtained using a Brucker (400MHz) spectrometer. Fourier transform. Fourier transform infrared (FTIR) spectra were examined using IR Prestige-21. The instruments used were Shimadzu 4000-400 cm^{-1}. Metals were identified using Shimadzu (F.A.A.) 680 G atomic clock. Magnetic properties were used with equilibrium magnetic susceptibility model MSR-MKI. All previous types of thermal analysis were performed using Perkin-Elmer Pyris Diamond DSC/TGA.

Synthesis of azo dye ligand: [7-(3-hydroxy-phenylazo)-quinoline-8-ol]

3-Aminophenol (1 g, 9.160 mmol) was dissolved in 15 mL of ethanol, 10 mL of distilled water under refrigeration at 5 °C was added. Then added 3 mL of concentrated HCl and (0.632 g, 9.160 mmol) $NaNO_2$ dissolved in cold distilled water was gradually added. After stirring the reaction for 45 min (1.32800 g, 9.160 mmol) of 8-hydroxyquinoline dissolved in 20 mL of ethanol was added to the diazonium salt. After stirring for 30 min for the reaction, the solution was observed to turn reddish brown. The product was collected after filtration and drying. The melting point was 162-165 °C, there was a brown precipitate, and the yield was 88%. Scheme 1 shows the formation of the azo dye ligand. It was then identified by proton and carbon nuclear magnetic resonance spectroscopy: the ^1H NMR and ^{13}C NMR spectra of the new azo dye are shown in Figure 1, showing the chemical shifts of these spectra; ^1H NMR δ 2.42-2.46-2.51 ppm (DMSO), 3.34 ppm (DHO), 7.51-7.93 ppm (2CH, m, 2H), 8.81-8.83-8.85 ppm (3CH (beside azo group), m, 3H), 10.25 ppm (OH-phenol, s, H), 10.48 ppm (OH-quinoline, s, H), respectively [11]; ^{13}C-NMR: 173.22 ppm (C1), 170.14 ppm (C5), 163.38 ppm (C10), 158.26 ppm (C8), 154.97 ppm (C9), 149.11 ppm (C7), 146.04 ppm (C13), 137.64 ppm (C12), 132.64 ppm (C3), 127.44 ppm (C11), 118.21 ppm (C15), 112.97 ppm (C14), 106.90 ppm (C2), 103.42 ppm (C4), 101.32 ppm (C6), 76.97 ppm (chloroform), respectively [12].

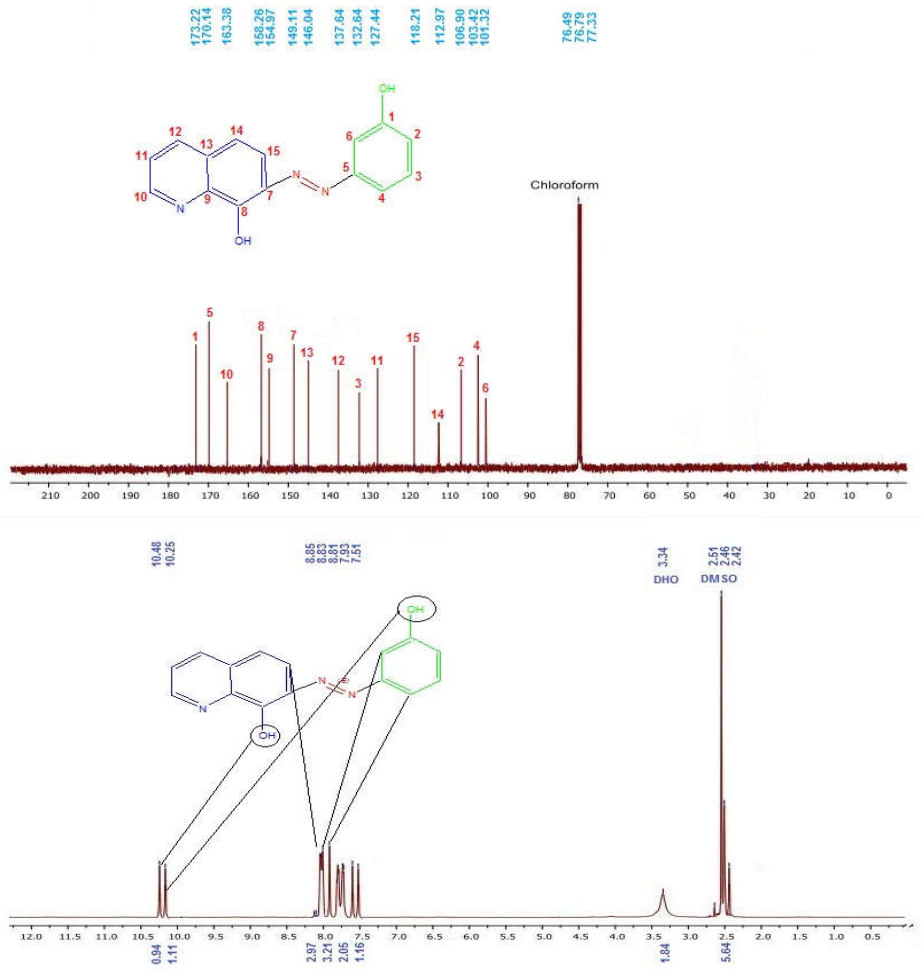

Figure 1. ^{13}C and ^{1}H-NMR spectra of ligand (H_2L).

General approach for synthesis of metal complexes

Dissolved 15 mL of azo ligand in hot ethanol (1 g, 0.00376 mmol), then added (0.3 g, 0.00752 mmol) from NaOH dissolved in water to the ligand and after 10 min of continuous stirring. The metal salt was added (0.00376 mmol) [$ZnCl_2$ (0.5), $CdCl_2$ (0.6), $FeCl_3$ (0.6), $CoCl_2.6H_2O$ (0.9)] was dissolved in 15 mL of water. The salts of [$RhCl_3.3H_2O$ (0.9) and $RuCl_3.3H_2O$ (0.9)] were dissolved in two drops of HCl and ethanol. Then the solutions were raised to the reverse osmosis for 6 hours at a temperature of 40 ºC. After completion, the solutions were raised and the solution was filtered while it was hot. The precipitate was collected and washed with a mixture of water and ethanol (1:1) and dried. It was then collected for analysis. The formation of the metal ion complex is Scheme 1.

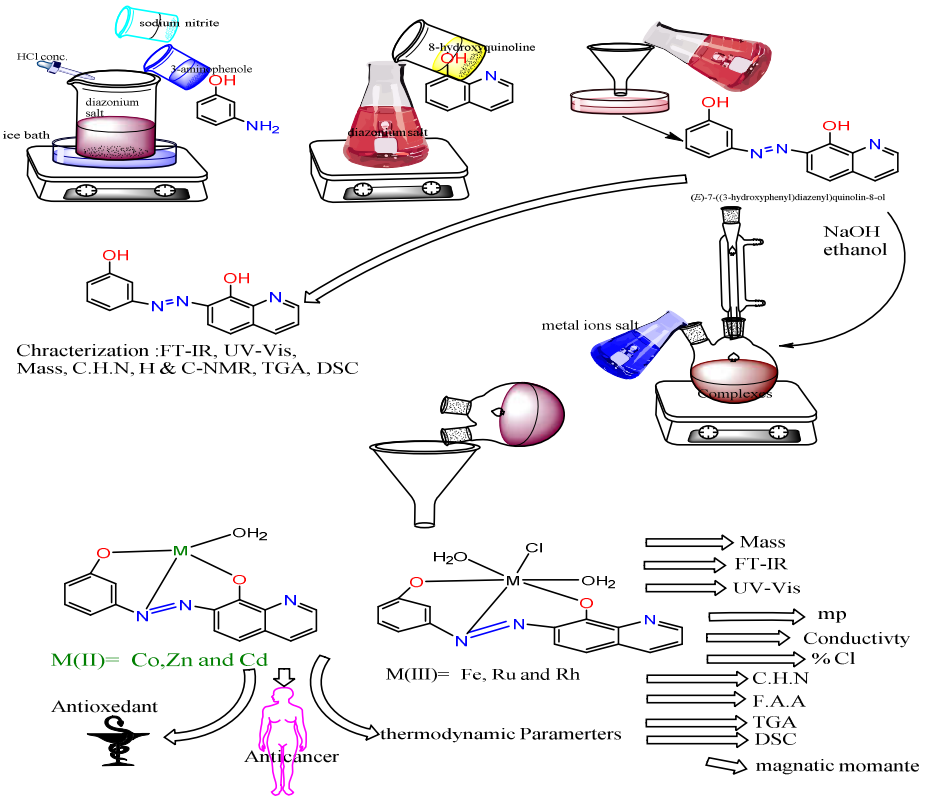

Scheme 1. Formation for the ligand (H_2L) and its metal complexes.

RESULTS AND DISCUSSION

Data on physical and analytical properties for the ligand and the synthesized complexes

The synthetic compounds illustrated in Scheme 1 were generated through the reaction of metal salts and ligand. Elemental analysis results indicate that all compounds exhibit a 1:1 M:L stoichiometry. These findings align with the theoretical calculations. Additionally, the conductivity measurements revealed that all the complexes are non-electrolytic, as shown in Table 1.

Table 1. Some elemental physical characteristics investigations of ligand and complexes.

Formula molecular weight	m.p. °C		C%	H%	N%	M%	Cl%	Conductivity in DMSO $cm^2\ \Omega^{-1}mol^{-1}$
$C_{15}H_{11}N_3O_2$ 265.27	165-167	Calculated	66.99	3.68	16.97	-	-	
		Found	67.09	4.18	15.84	-	-	
$C_{15}H_{11}N_3O_3Co$ 340.20	>300	Found	51.99	3.37	12.67	18.03	-	14
		Calculated	52.96	3.26	12.35	17.32	-	

$C_{15}H_{11}N_3O_3Zn$ 346.66	285-288	Found	52.48	4.01	13.11	17.96	-	11
		Calculated	51.97	3.20	12.12	18.86	-	
$C_{15}H_{13}N_3O_4ClRh$ 437.64	273-275	Found	40.94	3.64	10.59	-	9.03	20
		Calculated	41.17	2.99	9.60	-	8.10	
$C_{15}H_{13}N_3O_4ClRu$ 435.80	298-300	Found	42.10	2.38	10.44	-	7.88	13
		Calculated	41.34	3.01	9.64	-	8.14	
$C_{15}H_{13}N_3O_4ClFe$ 390.58	261-264	Found	45.67	3.67	11.05	13.94	10.01	19
		Calculated	46.13	3.35	10.76	14.30	9.08	

Ligand and some products in the LC mass spectrometry

One of the main methods used to characterize ligands (H_2L) and some products is LC mass spectrometry. This method complements other methods that use (m/z) relationships to estimate the molecular weight of chemicals [14]. Scheme 2 shows the mass information of the ligand and its complex, showing the fragmentation pattern and extracted mass for each mode [15]. The mass spectra of the ligand and its complexes are shown in Figure 2. The molecular ion peak of the $[M]^+$ fragment is clearly visible, $C_{15}H_{10}N_3O^+$. Its relative abundance is about 58% in Figure 2, in addition to the remaining peaks including other abundances of $C_6H_4^+$, $C_3H_2N_2O^+$ and $C_6H_5N_1^+$, corresponding to the abundances of 79%, 68%, 37%. For $[Fe(L)Cl(H_2O)_2]$ in Scheme 2, which illustrate the next fragments: (M^+) at 390.10 m/z with relative abundance 10% and next pattern: $C_{15}H_{10}ClFeN_3O_3^+$, $C_{15}H_9FeN_3O_3^+$, $C_{15}H_8FeN_3O_2^+$, $C_6H_3FeO^+$, $C_5H_3N^+$ and $C_3HN_2O^{+\cdot}$, which corresponded to 372.01 m/z, 336.67 m/z, 318.67 m/z, 147.22 m/z, 78.34 m/z, 81.14 m/z, respectively. For $[Zn(L)H_2O]$ complex in Scheme 2, which illustrate the next fragments: (M+) at 346.02 m/z with relative abundance 26% and next pattern: $C_{15}H_8N_3O_2Zn^+$, $C_6H_3NOZn^{\cdot+}$ and $C_9H_5N_2O^{\cdot+}$, which corresponded to 328.11 m/z, 157.22 m/z, 69.23 m/z, respectively. For the $[Rh(L)Cl(H_2O)_2]$ Scheme 2, which illustrate the next fragments: (M^+) at 437.12 m/z with a relative abundance of 37%, and the next patterns are $C_{15}H_{10}RhClN_3O_3$, $C_{15}H_8RhN_3O_2^+$, $C_6H_3N_2ORh^+$, and $C_9H_5NO^+$ which correspond to 419.01 m/z, 365.55 m/z, 222.11 m/z and 143.27 m/z, respectively [16, 17].

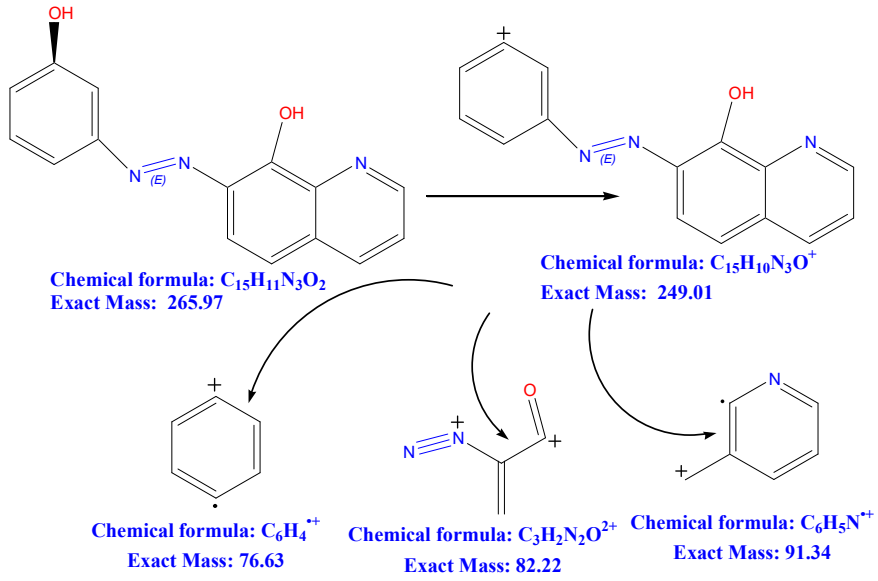

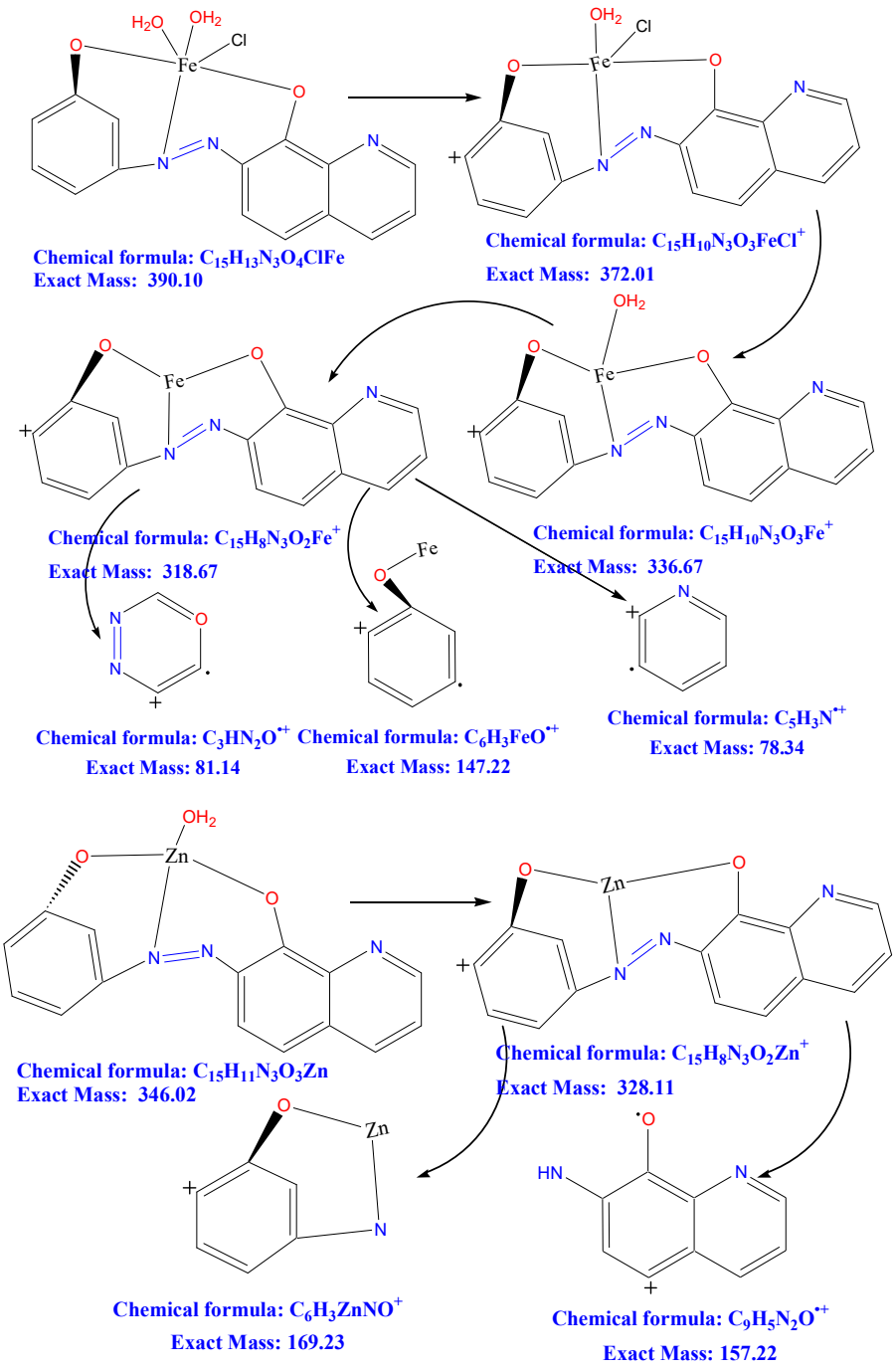
Chemical formula: $C_{15}H_{13}N_3O_4ClFe$
Exact Mass: 390.10
Chemical formula: $C_{15}H_{10}N_3O_3FeCl^+$
Exact Mass: 372.01
Chemical formula: $C_{15}H_8N_3O_2Fe^+$
Exact Mass: 318.67
Chemical formula: $C_{15}H_{10}N_3O_3Fe^+$
Exact Mass: 336.67
Chemical formula: $C_3HN_2O^{\bullet+}$
Exact Mass: 81.14
Chemical formula: $C_6H_3FeO^{\bullet+}$
Exact Mass: 147.22
Chemical formula: $C_5H_3N^{\bullet+}$
Exact Mass: 78.34
Chemical formula: $C_{15}H_{11}N_3O_3Zn$
Exact Mass: 346.02
Chemical formula: $C_{15}H_8N_3O_2Zn^+$
Exact Mass: 328.11
Chemical formula: $C_6H_3ZnNO^+$
Exact Mass: 169.23
Chemical formula: $C_9H_5N_2O^{\bullet+}$
Exact Mass: 157.22

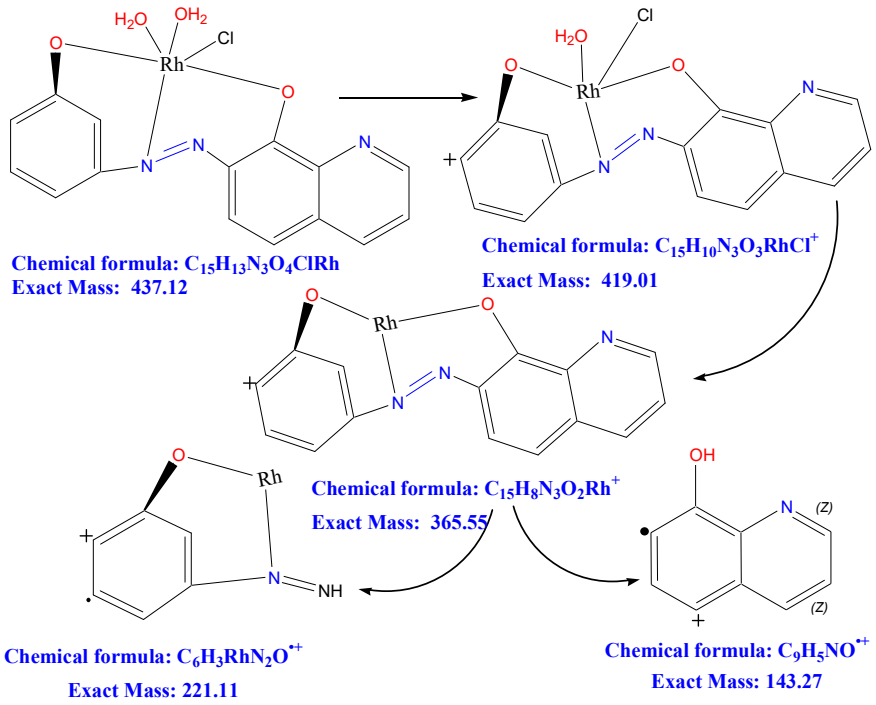

Scheme 2. Fragmentation of ligand, Fe-complex, Zn-complex and Rh-complex.

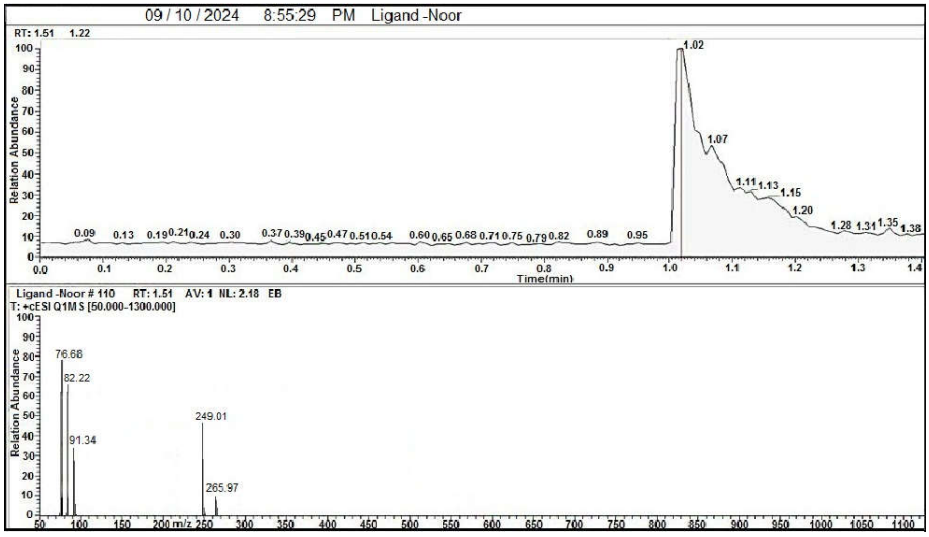

Mass spectrum of ligand

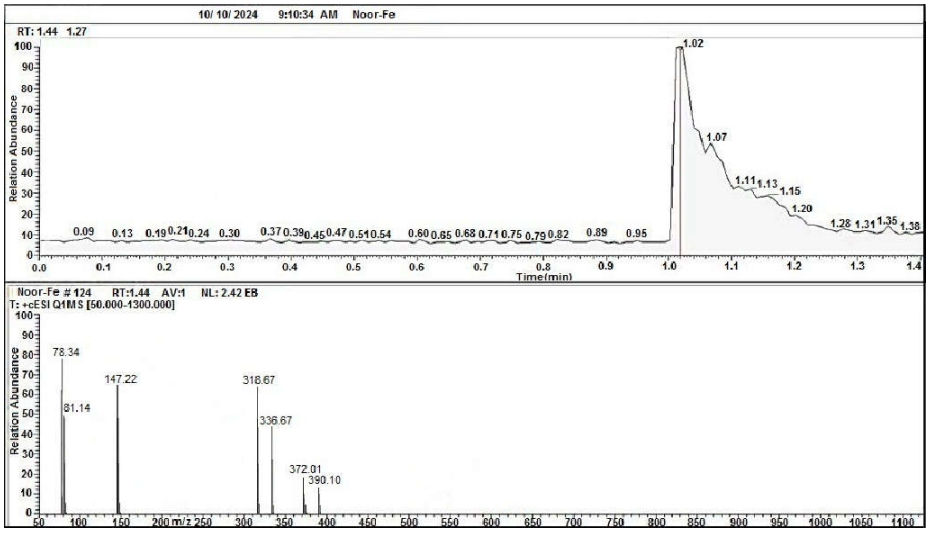

Mass spectrum of Fe-complex

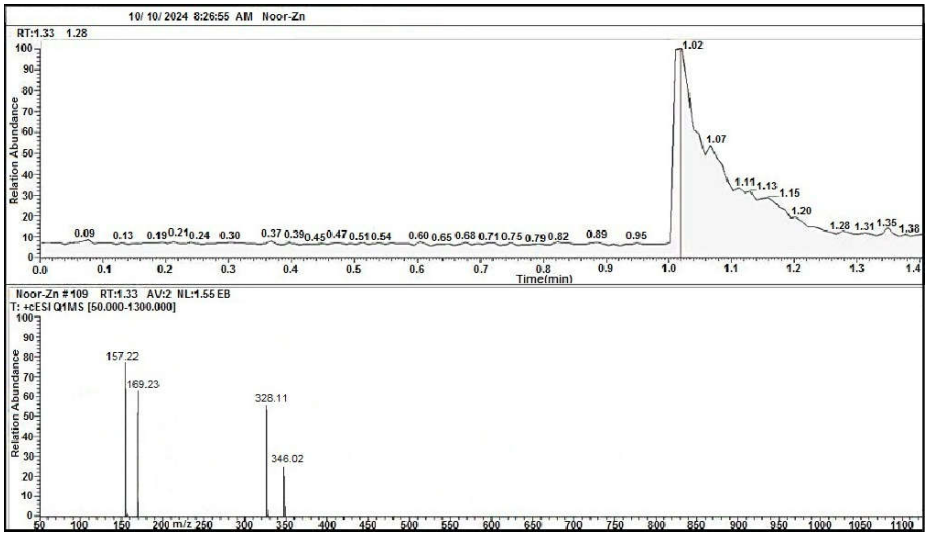

Mass spectrum of Zn-complex

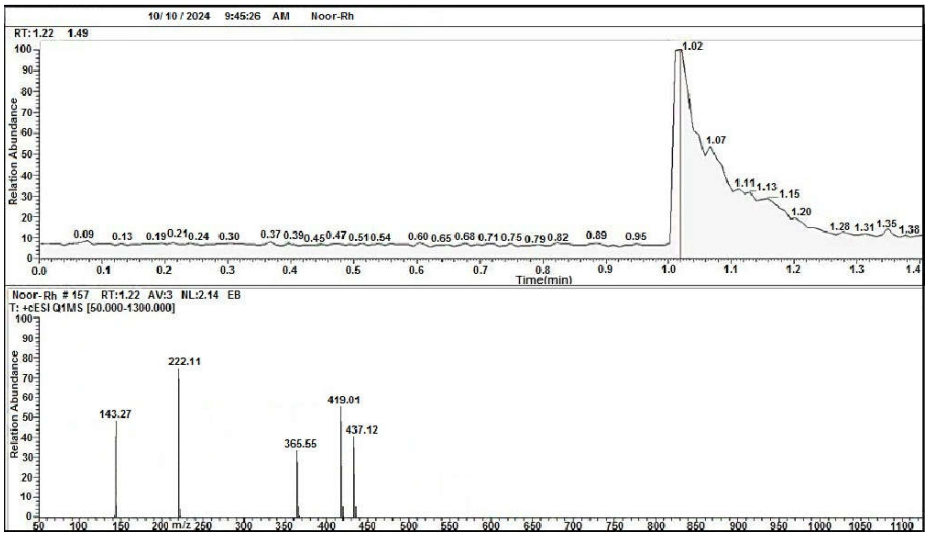

Mass spectrum of Rh-complex

Figure 2. Mass spectra of ligand, Fe-complex, Zn-complex, Rh-complex.

Electronic spectra for compound

The electronic spectrum of the ligand (H_2L) in Table 2 shows a strong absorption at (268 nm, 37313.43 cm^{-1}) due to the π→π* transition and a peak at (378 nm, 26455.02 cm^{-1}) attributed to the n→π* transition, where a high intensity band is formed with an absorption maximum [18]. The electronic spectrum of the Zn^{+2} complex show in Table 2 was studied, and it was found that it does not give d-d transitions because it contains (d^{10}) in the valence shell, but it gave four peaks, each belonging to the ligand spectrum, a peak at (221, 257, 272 and 408 nm) assigned to π→π*, π→π*, n→π*and C.T. M→L, respectively which is an indicative of a tetrahedral. The electronic spectrum of the Cd^{+2} show in Table 2 compound was studied, and it was found that it does not give d-d transitions because it contains (d^{10}) in the valence shell, but it gave two peaks, each belonging to the ligand spectrum, a peak at (264 and 413) nm assigned to π→π*, n→π* + C.T. M→L, respectively which is an indicative of a tetrahedral [20]. The electronic transition of Fe^{+3} complex show in Table 2 exhibited peaks at (277, 482, 550 and 648) nm assigned to π→π*, n→π*, $^6A_1g \rightarrow {}^4Eg(G)$ and $^6A1g \rightarrow {}^4T_2g(G)$, respectively, which indicative of an octahedral geometry. The electronic absorption of Co^{2+} complex show in Table 2 exhibited peaks at (212, 262, 622 and 763) nm ascribed to the π→π*, n→π*, $^4A_{2(F)} \rightarrow {}^4T_{2(F)}$ and $^4A_{2(F)} \rightarrow {}^4T_{1(P)}$, respectively, which is an indicative of a tetrahedral. The electronic transition of Rh^{+3} complex show in Table 2 is which depicts a peak at (259, 392, 588 and 610) nm ascribed to the π→π*, n→π*+C.T., $^6A1g \rightarrow {}^4T_1g(G)$ and $^6A_1g \rightarrow {}^4T_2g(G)$, respectively, it depicts an octahedral geometry. The electronic spectrum of the Ru^{+3} complex show in Table 2 was studied, exhibits peak at (260, 322, 435, 600 and 890) nm assigned to π→π*, n→π*, C.T., $^1A_1g \rightarrow {}^1T_1g$ and $^1A_1g \rightarrow {}^1T_2g$, respectively, it depicts an octahedral geometry [19-23] as shown in Table 2.

Table 2. The ligand and its complexes are studied by UV-Vis.

Compound	λ nm	νcm^{-1}	Abs	ε_{max}Lmol^{-1} cm^{-1}	Assignment	μ_{eff} (B.M.)	Hybridization	Distribution
Ligand	268	37313.43	2.03	2030	π→π*			
	378	26455.02	1.72	1720	n→ π*			
	424	23584.91	1.98	1980	C.T. (L→L)			
[Zn(L)H_2O] Tetrahedral	221	45248.86	0.538	538	π→π*	Diamagnetic	sp^3	$e^4 t_2^6$
	257	38910.50	0.485	485	π→π*			
	272	36764.70	0.478	478	n→π*			
	408	24509.80	0.342	342	C.T. M→L			
[Cd(L)H_2O] Tetrahedral	264	37878.78	0.483	483	π→π*	Diamagnetic	sp^3	$e^4t^4_2$
	413	24213.07	0.342	342	n→π*C.T. M→L			
[Fe(L)Cl(H_2O)$_2$] Octahedral	277	36101.08	1.268	1268	π→π*	5.801	sp^3d^2	$t_2g^3eg^2$
	482	20746.88	0.015	15	n→ π*			
	550	18181.81	0.018	18	$^6A_1g\rightarrow{}^4Eg(G)$			
	648	15432.09	0.023	23	$^6A1g\rightarrow{}^4T_2g(G)$			
[Co(L)H_2O] Tetrahedral	212	47169.81	1.182	1182	π→π*	3.658	sp^3	$e^4 t_2^3$
	262	38167.93	2.178	2178	n→π*			
	622	16077.17	0.021	21	$^4A_{2(F)}\rightarrow{}^4T_{2(F)}$			
	763	13106.15	0.025	25	$^4A_{2(F)}\rightarrow{}^4T_{1(P)}$			
[Rh(L)Cl(H_2O)$_2$] Octahedral	259	38610.03	1.555	1555	π→π*	Diamagnetic	d^2sp^3	$t_2g^6eg^0$
	392	25510.20	0.343	343	n→π*+C.T.			
	588	17006.80	0.098	98	$^6A1g\rightarrow{}^4T_1g(G)$			
	610	16393.44	0.082	82	$^6A_1g\rightarrow{}^4T_2g(G)$			
[Ru(L)Cl(H_2O)$_2$] Octahedral	260	38461.53	1.351	1351	π→π*	1.663	d^2sp^3	$t_2g^5eg^0$
	322	31055.90	1.054	1054	n→π*			
	435	22988.50	0.055	1155	C.T.			
	600	16666.66	0.024	24	$^1A_1g\rightarrow{}^1T_1g$			
	890	11235.95	0.012	12	$^1A_1g\rightarrow{}^1T_2g$			

Thermal analysis

The detailed results of the thermal decomposition of the complexes (Fe^{+3}, Ru^{+3}) are shown in Table 3 and Scheme 3 shows the stages of decomposition and the DSC results are shown in Table 3 showing the values of ΔH, ΔS, ΔG. Table 4 shows the thermogravimetric analysis of the complexes (Fe^{+3}, Ru^{+3}). The results of thermogravimetric decomposition were interpreted according to Scheme 3, which resulted in the decomposition of the ligand in one stage, and the remainder was carbon, while the two complexes were decomposed in three stages. The first stage included the loss of the two water molecules, and the final remainder was the oxidation of the metal for both of them [24-29].

Table 3. DSC analysis of thermal decomposition for the ligand and several complexes.

Compound	T_{i} /°C	T_{f}/°C	Maximum temperature point °C	ΔH J/g	ΔS J	ΔG J	Type
H_2L	235.65	399.13	349.40	-22.66	-1.362	153.22	Endothermic
$C_{15}H_{13}N_3O_4ClFe$	262.32	276.00	252.72	-39.10	-2.821	673.82	Endothermic
	242.78	268.22	274.71	-35.45	-1.393	347.22	Endothermic
	274.01	288.47	285.09	-14.54	-0.127	21.66	Endothermic
$C_{15}H_{11}N_3O_4ClRu$	385.95	397.87	399.99	-5.87	-0.492	190.92	Endothermic

Table 4. TGA data of the ligand and some complexes.

Complex	Step	T_i/°C	T_f/°C	Weight mass loss%		Reaction
				Calculated	Found	
Ligand	1	157.26 °C	593.919 °C	95.4763%	95.1913%	$C_{14}H_{11}N_3O_2$
Calculated: 95.48%, Final = 4.524%, Estimated = 95.1913%, Final = 4.808%						
Fe-complex	1	54.68 °C	188.12 °C	9.217%	9.104%	$-3H_2O$
	2	197.07 °C	378.28 °C	52.358%	52.476%	$-2H_2O$
	3	392.39 °C	568.65 °C	18.946%	18.957%	-Cl, $C_8H_5N_2$ $-C_2O$ -FeO
Calculated: 80.52%, Final = 19.479%, Estimated: 80.537%, Final = 19.463%						
Ru-complex	1	68.46 °C	228.62 °C	16.406%	16.743%	$-2H_2O$ -Cl
	2	236.84 °C	348.83 °C	23.864%	23.060%	$C_6H_4N_2$
	3	319.13 °C	557.75 °C	32.831%	33.005%	$-C_9H_5NO$ -RuO
Calculated: 73.10% , Final = 26.90%, Estimated 72.81%, Final = 27.20%						

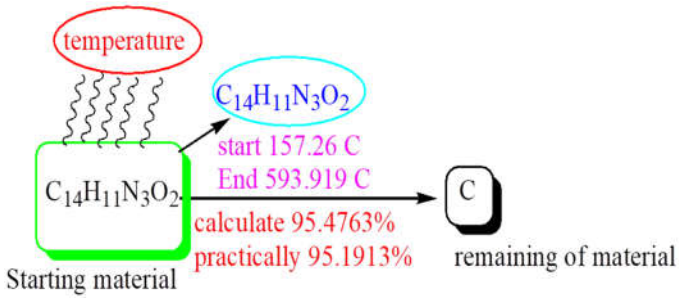

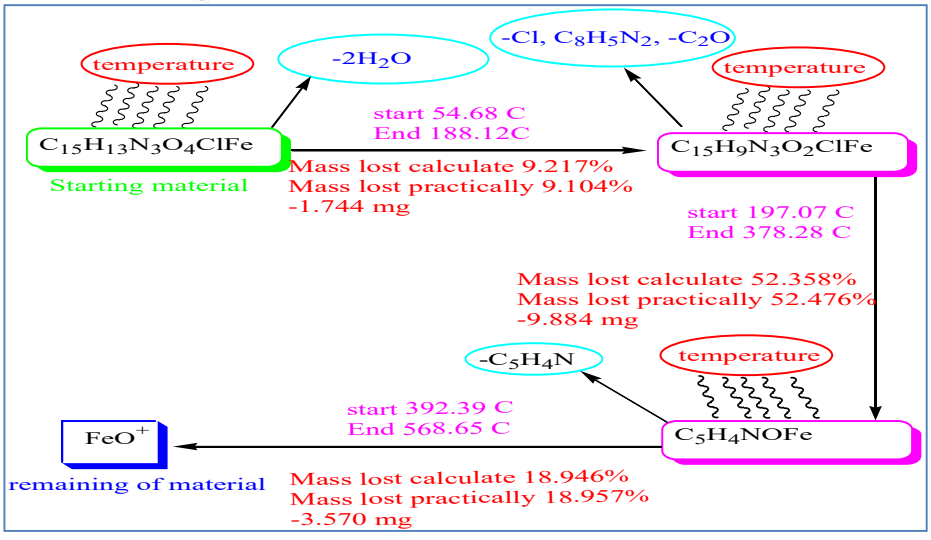

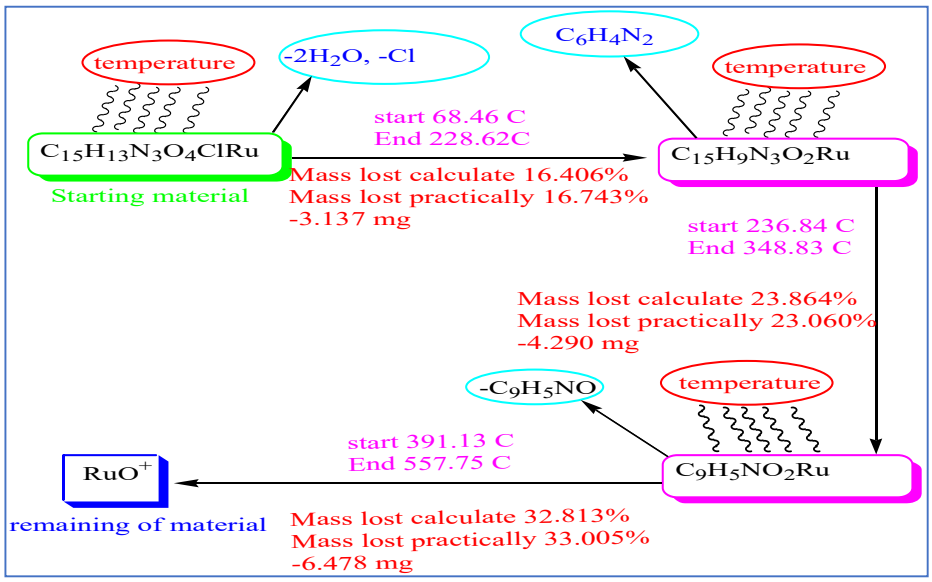

Scheme 3. Preliminary breakdown reactions of metal complexes and their ligand.

Infrared spectra

The infrared spectra of metal complexes were recorded with Fe^{+3}, Zn^{+2}, Cd^{+2}, Co^{+2}, Rh^{+3} and Ru^{+3} have been compiled, and show in Table 5 [24]. The ligand showed bands at 3051, 1139 cm^{-1} that were ascribed to the, ν(C-H) aromatic, ν(C-O). The infrared spectrum of the ligand showed a medium intensity stretch band at frequency 1381 cm^{-1}, which was attributed to the vibration frequencies of the double bond N=N [25]. After this, following this, the IR spectra of all the compounds created showed that the azo-dye ligand coupled to metal ions through two sites: the oxygen site via deprotonation of the phenolic group and the nitrogen site of the azo group. [26]. New bands belonging to (M-N) appeared at 588, 642, 609, 642, 613 and 559 cm^{-1} for the Fe^{+3}, Zn^{+2}, Cd^{+2}, Co^{+2}, Rh^{+3} and Ru^{+3}complexes, respectively, M-O at 445, 428, 484, 428, 443 and 420 cm^{-1} for the Fe^{+3}, Zn^{+2}, Cd^{+2}, Co^{+2}, Rh^{+3} and Ru^{+3}complexe, respectively. It was observed that the band at 3328 belonging to the phenol group in the ligand in the free state when the coordination process with the metal occurred, disappeared. This is evidence of a coordination process between oxygen and metal [27].

Antioxidant activity

The antioxidant activity of H_2L and its mineral complexes was measured by gallic acid and the DPPH assay was used to scavenge free radicals. Each sample was first diluted with the same volume of methyl alcohol and then combined with the same volume of concentrated 0.135 mM DPPH solution. After adding the DPPH solution [30-35]. The samples were stored at room temperature in the dark for 30 min. The absorbance of each sample was then measured at 517 nm. The lower the IC_{50} value of the complex, the stronger its ability to inhibit free radicals compared to gallic acid, because the ligand is the strongest free radical inhibitor, followed by gallic acid, followed by cobalt complex, iron complex, zinc complex, cadmium complex and ruthenium [36]. The IC_{50} values were lower and the results were as follows H_2L > gallic acid > Co complex > Fe complex, Zn complex, Cd complex and Ru complex, shown in Table 6.

Table 5. Infrared spectral bands of ligand and their complexes (cm^{-1}).

Compound	ν(H_2O) aqua	ν(C-H) aromatic	ν(C-O)	ν N=N)	Other bands
H_2L	-	3051	1139	1381	
Fe-Complex	3417, 1635, 995	3081	1271	1429	588 (Fe-N) 445 (Fe-O)
Zn-Complex	3498, 1618, 831	3188	1265	1469	642 (Zn-N) 428 (Zn-O)
Cd- Complex	3444, 1600, 819	3055	1261	1471	609 (Cd-N) 484 (Cd-O)
Co- Complex	3388,1575, 866	3042	1286	1460	642 (Co-N) 428 (Co-O)
Rh- Complex	3400, 1612, 821	3119	1143	1408	613 (Rh-N) 443 (Rh-O)
Ru- Complex	3375, 1605, 831	3104	1282	1409	559 (Ru-N) 420 (Ru-O)

Table 6. The antioxidant results (P1%, RSA% and IC_{50}) of ligand and their metal complexes.

Compound	Concentration µg/mL	PI%	RSA%	IC_{50} µg/mL
Ligand	0.080	22.06	77.94	0.020
	0.040	47.99	52.01	
	0.020	56.16	43.84	
	0.010	64.95	35.05	
	0.005	70.71	29.29	
Gallic acid	0.080	18.73	81.27	0.021
	0.040	45.69	54.31	
	0.020	60.35	39.65	
	0.010	68.16	31.84	
	0.005	72.36	27.64	
Cd	0.080	30.43	69.57	0.029
	0.040	41.43	58.57	
	0.020	47.33	52.67	
	0.010	50.19	49.81	
	0.005	53.61	46.39	
Fe	0.080	24.43	75.57	0.024
	0.040	36.82	63.18	
	0.020	44.96	55.04	
	0.010	47.62	52.38	
	0.005	50.01	49.99	
Zn	0.080	11.36	88.64	0.025
	0.040	20.33	79.67	
	0.020	27.06	72.94	
	0.010	28.75	71.25	
	0.005	30.04	69.96	
Co	0.080	22.94	77.06	0.023
	0.040	25.91	74.09	
	0.020	27.11	72.89	
	0.010	29.14	70.86	
	0.005	30.41	69.59	
Ru	0.080	24.43	75.57	0.031
	0.040	36.82	63.18	
	0.020	46.03	53.97	
	0.010	48.12	51.88	
	0.005	50.66	49.34	

Table 7. Cellular toxicity of cobalt complex towards MCF7.

Control (untreated sample) average absorption at 570 nm = Co complex					
Sample ID	Concentration (µg/mL)	Absorption at 570 nm	Viability (%)	Average viability (%)	Standard deviation (±)
NAT-1 MCF 7 24 h	7.4	0.338	95.29	94.99	0.81
		0.329	94.69		
	22.22	0.320	92.65	92.33	0.64
		0.312	92.01		
	66.66	0.304	89.37	88.64	0.41
		0.301	87.91		
	200	0.296	86.05	84.49	2.31
		0.292	82.94		
	600	0.260	70.18	66.56	9.84
		0.224	62.94		
IC_{50} = 93.84 µg/mL		A = -0.045x	b = 93.50	R^2 = 0.986	
Control (untreated sample) average absorption at 570 nm = Zn complex					
Sample ID	Concentration (µg/mL)	Absorption at 570 nm	Viability (%)	Average viability (%)	Standard deviation (±)
NAT-6 MCF 7 24 h	7.4	0.286	83.55	84.71	0.83
		0.290	85.87		
	22.22	0.262	76.94	78.82	2.50
		0.274	80.70		
	66.66	0.133	68.28	69.53	0.83
		0.129	70.78		
	200	0.063	35.97	37.68	0.21
		0.064	39.39		
	600	0.049	11.67	10.12	0.42
		0.047	8.57		
IC_{50} = 43.38 µg/mL		a= -0.121x	b = 77.98	R^2 = 0.911	
Control (untreated sample) average absorption at 570 nm = Ru					
Sample ID	Concentration (µg/mL)	Absorption at 570 nm	Viability (%)	Average viability (%)	Standard deviation (±)
NAT-2 MCF 7 24 h	7.4	0.338	91.29	92.67	0.82
		0.326	94.05		
	22.22	0.325	88.61	87.98	0.63
		0.317	87.35		
	66.66	0.307	82.67	84.64	0.39
		0.305	86.61		
	200	0.288	78.94	77.67	2.31
		0.292	76.40		
	600	0.257	66.23	64.67	9.84
		0.226	63.11		
IC_{50} = 63.57 µg/mL		A = -0.042x	b = 89.19	R^2 = 0.942	

Investigation of anticancer activity

Cancer cell growth was determined using MTT, and MCF7 cells were digested with trypsin. The cells were treated with 7.4-600 µg/mL (five concentration) with compounds for 24 hours at 37 °C in 5% CO_2, and the MTT solution was added in phosphate-buffered saline for an additional four hours, and the absorbance was determined as 570 nm. Using an ELISA reader, and the concentration of compounds Co-Complex, Zn-Complex, Ru-Complex in Table 7, that led to 50% of cell death was determined, the results showed that the inhibition was high for the complexes, as the highest inhibition was for zinc, followed by ruthenium and cobalt according to the IC value.

When compared to healthy cells. Also, the percentage of free radical inhibition of these compounds was cobalt, which gave the highest inhibition, followed by zinc, then ruthenium. These complexes were chosen over others based on studies and references that advise preferring these minerals over others due to their vital importance. [37-42].

CONCLUSION

In summary, using a straightforward substitution process using 8-hydroxyquinoline, we were able to successfully synthesize a novel azo ligand derivative with 3-amino phenol. Then, ligand and metal the complexes were identified using various analytical methods, including thermal analysis curves (TGA and DSC), elemental microanalysis, metal chlorides, conductivity measurements, magnetic susceptibility, ^{1}H and ^{13}C NMR, FT-IR and UV-Vis spectroscopy. Thermodynamic parameters ΔH, ΔS and ΔG were calculated using DCS curves. The tridentate coordination sites of atoms N, O and O in the ligand were identified by comparing the infrared spectra with those of the metal complexes. The M:L ratio of each compound was [1:1]. The dye was used to determine its ability to inhibit free radicals using its prepared complexes, and its ability as an antioxidant was determined using DPPH as a free radical and gallic acid as a standard substance, The IC_{50} value was determined and it was found that the ligand had a high free radical inhibition ability. The free radical inhibition ability and complex inhibition ability changed according to the IC_{50} value, and the results were as follows (H_2L > gallic acid > Co complex > Fe complex > Zn complex > Cd complex > Ru complex).

REFERENCES

1. Mohammed, H.S. Synthesis, characterization, structure determination from powder X-ray diffraction data, and biological activity of azo dye of 3-aminopyridine and its complexes of Ni(II) and Cu(II). *Bull. Chem. Soc. Ethiop*. **2020**, 34, 523-532.
2. Dakiky, M.; Nemcova, I. Aggregation of o,o′-dihydroxy azo dyes III. Effect of cationic, anionic and non-ionic surfactants on the electronic spectra of 2-hydroxy-5-nitrophenylazo-4-[3-methyl-1-(4 ″-sulfophenyl)-5-pyrazolone], *Dyes Pigm*. **2000**, 44, 181-193.
3. Mezgebe, K.; Mulugeta, E. Synthesis and pharmacological activities of azo dye derivatives incorporating heterocyclic scaffolds. A review. *RSC Adv*. **2022**, 12, 25932-25946.
4. Reda, S.M.; Al-Hamdani, A.A.S. Synthesis, characterization, thermal analysis and bioactivity of some transition metals complexes with new azo ligand. *Chem. Methodol*. **2022**, 6, 475-493.
5. Al-Resayes, S.I.; Jarad, A.J.; Al-Zinkee, J.M.; Al-Noor, T.H.; El-ajaily, M.M.; Abdalla, M.; Min, K.; Azam, M.; Mohapatra, R.K. Synthesis, characterization, antimicrobial studies, and molecular docking studies of transition metal complexes formed from a benzothiazole-based azo ligand. *Bull. Chem. Soc. Ethiop*. **2023**, 37, 931-944.
6. Al Zoubi, W.; Jirjees, V.; Suleman, V.; Kim, Y.G.; Ko, Y.G. Synthesis and bioactivity studies of novel Schiff bases and their complexes. *J. Phys. Org. Chem*. **2019**, 32, e4004.
7. Patra, A.K.; Nethaji, M.; Chakravarty, A.R. Synthesis, crystal structure, DNA binding and photo-induced DNA cleavage activity of (S-methyl-l-cysteine) copper(II) complexes of heterocyclic bases. *J. Inorg. Biochem*. **2007**, 101, 233-244.
8. Nakbi, H.; Dallel, W.; Hammami, S.; Mighri, Z. Phytochemical profile and antioxidant properties of leaves extracts from *Posidonia oceanica* (L.) Delile and their allelopathic potential on terrestrial plant species. *Bull. Chem. Soc. Ethiop*. **2020**, 34, 437-447.
9. Hirano, R.; Sasamoto, W.; Matsumoto, A.; Itakura, H.; Igarashi, O.; Kondo, K. Antioxidant ability of various flavonoids against DPPH radicals and LDL oxidation. *J. Nutr. Sci. Vitaminol*. **2001**, 47, 357-362.
10. Mohammed, H.; Al-Hasan, H.; Chaieb, Z.; Zizi, Z.; Abed, H. Synthesis, characterization, DFT calculations and biological evaluation of azo dye ligand containing 1,3-dimethylxanthine and

its Co(II), Cu(II) and Zn(II) complexes. *Bull. Chem. Soc. Ethiop*. **2023**, 37, 347-356.
11. Jirjees, V.Y.; Al-Hamdani, A.A.S.; Wannas, N.M.; Dib, A.; Al Zoubi, W. Spectroscopic characterization for new model from Schiff base and its complexes. *J. Phys. Org. Chem.* **2021**, 34, e4169.
12. Zafar, S.; Bukhari, D.A.; Rehman, A. Azo dyes degradation by microorganisms–An efficient and sustainable approach. *Saudi J. Biol. Sci*. **2022**, 29, 103437.
13. Shahi, N.; Shah, S.K.; Yadav, A.P.; Bhattarai, A. Micellization pattern of cationic surfactants in presence of azo dye in methanol mixed media. *Results Chem*. **2023**, 5, 100906.
14. Alhalafi, M.H. Novel azo-dye quinazolinones as colorimetric chemosensors for detection of cobalt and ferrous ions in aqueous medium. *J. Saudi Chem. Soc*. **2023**, 27, 101685.
15. Ravi, B.N.; Keshavayya, J.; Kumar, V.; Kandgal, S. Synthesis, characterization and pharmacological evaluation of 2-aminothiazole incorporated azo dyes. *J. Mol. Struct*. **2020**, 1204, 127493.
16. Agwamba, E.C.; Udoikono, A.D.; Louis, H.; Udoh, E.U.; Benjamin, I.; Igbalagh, A.T.; Ushaka, U.B. Synthesis, characterization, DFT studies, and molecular modeling of azo dye derivatives as potential candidate for trypanosomiasis treatment. *Chem. Phys. Impact* **2022**, 4, 100076.
17. Asiri, S.; Kassem, M.A.; Eltaher, M.A.; Saad, K.M. Novel coordination compounds based on copper complexes with new synthesized Schiff bases and azo-dyes as sensitizers for dye-sensitized solar cells: Spectral and electrochemical studies. *Int. J. Electrochem. Sci*. **2020**, 15, 6508-6521.
18. Obaid, S.M.H.; Jarad, A.J.; Salih Al-Hamdani, A.A. Synthesis, characterization and biological activity of mixed ligand metal salts complexes with various ligands. *J. Phys.: Conf. Ser*. **2020**, 1660, 012028.
19. Venugopal, N.; Krishnamurthy, G.; Bhojyanaik, H.S.; Krishna, P.M. Synthesis, spectral characterization and biological studies of Cu(II), Co(II) and Ni(II) complexes of azo dye ligand containing 4-amino antipyrine moiety. *J. Mol. Struct*. **2019**, 1183, 37-51.
20. Prashantha, G.; Keshavayya, J.; Ali, R.S. Synthesis, spectral characterizations and biological applications of novel 3-[(E)-(4,6-dihydroxy pyrimidin-5-yl) diazenyl]-4-methylbenzoic acid azo dye and their derivatives. *Results Chem*. **2021**, 3, 100110.
21. Mohamed Wannas, N.; Al-Hamdani, A.A.S.; Al Zoubi, W. Spectroscopic characterization for new complexes with 2,2′-(5,5-dimethylcyclohexane-1,3-diylidene)bis(azan-1-yl-1-ylidene)dibenzoic acid. *J. Phys. Org. Chem*. **2020**, 33, e4099.
22. Akram, D.; Elhaty, I.A.; AlNeyadi, S.S. Synthesis and spectroscopic characterization of rhodanine azo dyes as selective chemosensors for detection of iron(III). *Chem. Data Collect*. **2020**, 28, 100456.
23. Al Zoubi, W.; Al-Hamdani, A.A.S.; Widiantara, I.P.; Hamoodah, R.G.; Ko, Y.G. Theoretical studies and antibacterial activity for Schiff base complexes. *J. Phys. Org. Chem*. **2017**, 30, e3707.
24. Hussain Al-Daffay, R.K.; Salih Al-Hamdani, A.A. Synthesis and characterization of some metals complexes with new acidicazo ligand 4-[(2-amino-4-phenylazo)-methyl]-cyclohexane carboxylic acid. *Iraqi J. Sci*. **2022**, 63, 3264-3275.
25. Abd El-Lateef, M.; Khalaf, M.; Amer, A.; Kandeel, M.; Abdelhamid, A.; Abdou, A. Synthesis, characterization, antimicrobial, density functional theory, and molecular docking studies of novel Mn(II), Fe(III), and Cr(III) complexes incorporating 4-(2-hydroxyphenylazo)-1-naphthol (Az). *ACS. Omega* **2023**, 8, 25877-25891.
26. El-Ghamry, H.A.; Alkurbi, A.A.; Alhasani, M.A.; Takroni, K.M.; Khedr, A.M. Copper-based azo dye catalysts for phenoxazinone synthase mimicking efficiency: structure characterization and bioactivity evaluation. *Arab. J. Chem*. **2023**, 16, 104916.
27. Ren, H.; Li, F.; Yu, S.; Wu, P. The detection of multiple analytes by using visual colorimetric and fluorometric multimodal chemosensor based on the azo dye. *Heliyon* **2022**, 8, 1-12.

28. El-Ghamry, H.A.; Alkurbi , A.A.; Alhasani, M.A.; Takroni, K.M.; Khedr, A.M. Copper based azo dye catalysts for phenoxazinone synthase mimicking efficiency structure characterization and bioactivity evaluation. *Arab J. Chem*. **2023**, 16, 104916,
29. Al-Hamdani, A.A.S.; Al-Zahraa, F.SH.H.; Mutar, S.A.; Mohammed, N.U.G. Synthesis and characterization of new (Au, Ru and Rh) ion complexes and evaluating their activity as anticancer and antioxidants. *Appl. Biochem. Biotechnol.* **2025**, DOI: 10.1007/s12010-024-05140-w.
30. Al-Daffay, R.K.H.; Al-Hamdani, A.A.S. Synthesis, characterization, and thermal analysis of a new acidicazo ligand's metal complexes. *Baghdad Sci. J*. **2023**, 20, 121-133.
31. Keshavayya, J. Synthesis, structural investigations and in vitro biological evaluation of N,N-dimethyl aniline derivatives based azo dyes as potential pharmacological agents. *J. Mol. Struct*. **2019**, 1186, 404-412.
32. Obaid, S.M.H.; Sultan, J.S.; Al-Hamdani, A.A.S. Synthesis, characterization and biological efficacies from some new dinuclear metal complexes for base 3-(3,4-dihydroxy-phenyl)-2-[(2-hydroxy-3-methylperoxybenzylidene)-amino]-2-methyl propionic acid. *Indones. J. Chem.* **2020**, 20, 1311-1322.
33. Reda, M.M.; Mohammed, L.A. Preparation, characterization and studied biological effect as antioxidant of azo compound and Schiff base complexes. *J. Surv. Fish. Sci*. **2023**, 10, 1144-1156.
34. Sarvalkar, P.D.; Jamadar, A.S.; Magdum, A.B.; Pawar, P.K.; Yadav, J.B.; Nimbalkar, M.S.; Sharma, K.K. Biogenic synthesis of Co_3O_4 nanoparticles from Aloe barbadensis extract: Antioxidant and antimicrobial activities, and photocatalytic degradation of azo dyes. *Results Eng*. **2024**, 22, 102094.
35. Hamza, I.S.; Mahmmoud, W.A.; Al-Hamdani, A.A.; Allaf, A.W.; Al Zoubi, W. Synthesis, characterization, and bioactivity of several metal complexes of (4-Amino-N-(5-methyl-isaxazol-3-yl)-benzenesulfonamide). *Inorg. Chem. Commun*. **2022**, 144, 109776.
36. Jirjees, V.Y.; Suleman, V.T.; Al-Hamdani, A.A.S.; Ahmed, S.D. Preparation, spectroscopic characterization and theoretical studies of transition metal complexes with 1-[(2-(1H-indol-3-yl)ethylimino)methyl]naphthalene-2-ol ligand. *Asian J. Chem*. **2019**, 31, 2430-2438.
37. Reda, S.M.; Al-Hamdani, A.A.S. Mn(II), Fe(III), Co(II) and Rh(III) complexes with azo ligand: Synthesis, characterization, thermal analysis and bioactivity. *Baghdad Sci. J*. **2023**, 20, 642-660.
38. Al-Hamdani, A.A.S.; Al Zoubi, W. Synthesis, spectral studies and biological activity. *Spectrochim. Acta. Part A* **2015**, 137, 75-89.
39. Hekal, H.A.; Kassab, R.M.; Abd El Salam, H.A.; Shaban, E.; Atlam, F.M. Synthesis, computational studies, molecular docking, anti-inflammatory and antioxidant activities of α-aminophosphonates incorporating an azo chromophore for polyester printing application. *ChemistrySelect* **2023**, 8, e202204075.
40. Al-Zahraa, F.S.H.H.; Al-Hamdani, A.A.S. Synthesis, characterization, thermal studies, and antioxidant activities of azo dye [2-[(3-hydroxyphenyl)diazinyl]-1,2-benzothiazol-3(2H)-one-1,1-dioxide] and metal ion complexes. *Iraqi J. Sci*. **2024**, 65, 6842-6861.
41. Fadhel, A.M.; Al-Hamdani, A.A.S.; Mohamed, S.G. Synthesis, characterization and antioxidant study of some metal ion complexes with azo 1-(2,4,6-trihydroxy-3-((3-hydroxyphenyl) diazenyl) phenyl) ethan-1-one. *Baghdad Sci. J*. **2024**, 21, 3642-3660.
42. Abdullah, A.M.; Al-Hamdani, A.A.S. Synthesis, characterization, thermal studies and antioxidant activities of transition metal complexes with azo dye ligand. *Baghdad Sci. J.***2024**, 21, 1512-1535.